# Comparative Proteomic Analysis of Bleomycin-induced Pulmonary Fibrosis Based on Isobaric Tag for Quantitation

Tiejun Yang, MS, Yanlong Jia, MD, Yongkang Ma, MS, Liang Cao, MS, MD, Xiaobing Chen, MD and Baoping Qiao, MD

## ABSTRACT

**Background:** Pulmonary fibrosis (PF) is a destructive pulmonary disease and the molecular mechanisms underlying PF are unclear. This study investigated differentially expressed proteins associated with the occurrence and development of PF in rat lung tissue with bleomycin-induced PF.

**Methods:** Sixteen Sprague-Dawley rats were randomly divided into 2 groups: the PF model group ($n = 8$) and the control group ($n = 8$). After successfully establishing the rat PF model induced by bleomycin, the differentially expressed proteins in the 2 groups were identified through isobaric tag for relative and absolute quantitation coupled with liquid chromatography-mass spectrometry and bioinformatics analysis.

**Results:** A total of 146 differentially expressed proteins were identified; 88 of which displayed increased abundance and 58 were downregulated in the PF rat model group. Most functional proteins were associated with extracellular matrix, inflammation, damage response, vitamin A synthesis and metabolism. Critical proteins related to PF development and progression was identified, such as type V collagen-3, arachidonic acid 12-lipoxygenase, arachidonic acid 15-lipoxygenase and cytochrome P4501A1. Kyoto Encyclopedia of Genes and Genomes pathway analysis showed that these differentially expressed proteins were enriched in extracellular matrix receptor interaction pathway, renin-angiotensin system and metabolic pathway of retinol.

**Conclusions:** The proteins expressed in bleomycin-induced PF rat model provide important data for further functional analysis of proteins involved in PF.

**Key Indexing Terms:** Pulmonary fibrosis; Proteome; Bleomycin; Isobaric tag for relative and absolute quantitation; Rat model. **[Am J Med Sci 2017;353(1):49–58.]**

## INTRODUCTION

Pulmonary fibrosis (PF) is a destructive pulmonary disease caused by the accumulation of fibroblasts and deposition of extracellular matrix (ECM). In recent years, the incidence of PF has significantly increased and represents a serious threat to public health.[1,2] The etiology of PF is still unknown,[3] and its early diagnosis is difficult.[4] In addition, the survival time after diagnosis is very short, and its prognosis is very poor.[5] The survival time of approximately 50% of the patients after diagnosis is only 5 years.[6] Currently, the pathogenesis of PF is unclear, and a breakthrough in early prevention and treatment is desirable. Therefore, it is imperative to explore the molecular mechanisms underlying PF.

The role of inflammation, especially cytokines, in PF has been identified in some studies.[7,8] However, inflammation is not a prerequisite for the development of PF; fibrosis still occurs in alveolar epithelial cells in the absence of inflammation.[9] A few studies analyzed the molecular mechanism of PF at the genetic level and signal transduction pathways.[10] Factors mediating PF have yet to be elucidated.

In recent years, application of isotope-labeling measuring techniques has improved the detection rate of peptide fragments in protein identification. This technique with good reproducibility provides accurate and reliable quantitative results.[11] It is an effective supplement to label-free quantitative proteomics[12] and is especially suitable for quantitative differential analysis of proteomics at multiple time points during physiological and pathologic processes. It is used to monitor the dynamic changes of key protein molecules, and it enables important regulatory targets to be easily explored. In this study, we detected and analyzed differentially expressed proteins (DEPs) in lung tissues of the model and control groups by isobaric tag for relative and absolute quantitation (iTRAQ) combined with liquid chromatography-mass spectrometry (LC-MS-MS). We investigated the key proteins related to PF and provided new targets for the origin and development as well as diagnosis, prevention and treatment of PF.

## MATERIALS AND METHODS

### Establishment of Rat Model With Bleomycin-Induced PF

The study was approved by the Animal Care Committee of the First Affiliated Hospital of Zhengzhou University (No. ZZU-FAH-2010-086) and conducted according to the Guidelines for Animal Experiments. Sixteen 6-8-week-old male Sprague-Dawley rats weighing 180 g to 200 g each were obtained from the Henan Experimental Animal Center, license No.: SCXK (Yu) 2010-0002 and were randomly divided into 2 groups: bleomycin-induced PF (model group) and control. Anesthesia was induced by an intraperitoneal injection of 10% chloral hydrate (300 mg/kg). The neck skin was disinfected and incised. Rats in the model group received a single intratracheal instillation of 0.2 mL bleomycin hydrochloride A5 (Nippon Kayaku Co. Ltd., batch number: Y32480) solution (5 mg/kg) to induce PF as previously described.[13] Rats were immediately shifted to an upright position and rotated to distribute the drugs uniformly as much as possible to replicate a bleomycin-induced PF model. In the control group, rats were administered an intratracheal injection of 0.2 mL saline similarly. Animals were transferred back to the cage and raised routinely. Rats in both the groups were sacrificed on day 28 after the administration. Bilateral lung tissues were completely isolated from each rat and weighed. The left lung tissue was fixed with 4% neutral formalin, which was collected after 16 hours, embedded in paraffin and sectioned. Subsequently, rats were stained with hematoxylin-eosin to determine the degree of pulmonary alveolitis. The remainder of the sample tissues were preserved in liquid nitrogen.

### Determination of Alveolar Inflammation and PF in Rats

After hematoxylin-eosin staining of the paraffin-embedded section, the pathologic changes of the left lung tissue were observed microscopically. The degree of alveolitis and fibrosis was assessed by the method proposed by Szapiel et al.[14] The degrees of pulmonary alveolitis and fibrosis were classified into 4 grades: grade 0 refers to absence of significant pathologic changes and normal alveolar structure, with a score of 0; grade 1 refers to mild changes and a diseased area of less than 20% of the whole lung, with a score of 1; grade 2 refers to moderate changes and lesions ranging from 20-50% of the whole lung, with a score of 2; and grade 3 represents severe changes and a lesion area of greater than 50% of the whole lung, with a score of 3.

### Calculation of Lung Coefficient and Determination of Hydroxyproline Content

Bilateral lung tissues were completely isolated from rats and rinsed with saline. The water on the lung surface was soaked with filter paper, and the wet weight was accurately determined to calculate the lung coefficient. The lung coefficient was calculated by dividing lung wet weight (mg) by the body weight (g). The middle lobe of the right lung was weighed, cut into pieces and mixed. The hydroxyproline content was detected according to the method described in the hydroxyproline assay kit (Nanjing Jiancheng Bioengineering Co. Ltd., China).

### Extraction of the Total Protein From Lung Tissue

The preserved lung tissues of each group were ground into powder and stored in liquid nitrogen. The protein lysis buffer (7 M urea, 2 M citrol, 4% CHAPS, Protease Inhibitor Cocktail 50 mL/piece) was added to each sample powder (W/V: 1:10), followed by vortexing and ultrasonic (60 seconds, 0.2 seconds on, 2 seconds off and amplitude 22%) extraction at room temperature for 30 minutes, and centrifugation (15,000*g*, 10°C for 1 hour). The supernatant was collected, packaged and frozen at −80°C. The concentration of extracted protein was tested using the Bradford assay. The sample was diluted with the lysis buffer (7 M urea, 2 M citrol and 1% CHAPS) to obtain a final concentration within the range of the standard curve. BSA was dissolved to a series of standard protein concentrations with lysis buffer. A 10 μL diluted sample and standard product were collected separately, and reacted respectively, with 300 μL protein quantitation dye under dark for 20 minutes. The absorbance was read at 595 nm for the standard product and the sample using a microplate reader (Thermo, No. Multiskan MK3). The standard curve of the relationship between absorbance and concentration of the standard product in each tube was obtained, and the protein concentration of each sample was calculated.

### Enzymolysis of the Proteins

After protein quantification, 200 μg of the protein sample was collected from each tube for enzymolysis with isobaric tag for relative and absolute quantitation (iTRAQ) kit (AB Sciex, Framingham, MA), supplemented with 4 μL of reducing reagent for reaction at 60°C for 1 hour, followed by 2 μL cysteine-blocking reagent at room temperature for 10 minutes. After reductive alkylation, the protein solution was added to a 10K ultrafiltration device (Sartorious, Germany) and centrifuged at 12,000 rpm for 20 minutes. The solution at the bottom was discarded, followed by the addition of 100 μL dissolution buffer and centrifuged at 12,000 rpm for 20 minutes. The solution at the bottom was discarded, and the procedure was repeated 3 times. Subsequently, the collection tube was replaced. Trypsin (AB Sciex, Framingham, MA) 4 μg (mass ratio to protein: 1:50) in a volume of 50 μL was added to the ultrafiltration device, and reacted at 37°C overnight. The next day, the sample was centrifuged at 12,000 rpm for 20 minutes. The peptide segments after enzymatic digestion were retained at the bottom of the collection tube followed by addition of 50 μL dissolution buffer to the ultrafiltration

device and centrifuged at 12,000 rpm for 20 minutes. A 100 μL of enzymatic sample was collected from the bottom of the collection tube.

### Labeling With iTRAQ

iTRAQ kit (AB Sciex, Framingham, MA) was removed from the freezer and restored to room temperature. Isopropanol (150 μL) was added to iTRAQ reagent in each tube, vortexed and centrifuged. Next, a 50 μL sample (100 μg hydrolysate) was transferred to a new centrifuge tube. After addition of iTRAQ reagent (labeled reagents 114 and 115 corresponding to the control and model groups, respectively) and vortexing and centrifugation at room temperature for 2 hours, 100 μL of double-distilled water was used to terminate the reaction. The labeling efficiency and quantitative accuracy were verified in 1 μL samples of both groups. They were mixed and demineralized with Ziptip (Millipore), followed by mass spectrometry using MALDI-TOF-TOF (ABSCIEX 4800Plus). The labeled samples were mixed, vortexed and centrifuged, followed by vacuum freezing and centrifugal drying for subsequent experiments.

### Offline Predissociation of Enzymatic Peptides and LC-MS-MS Mass Analysis

Labeled samples were mixed, dissolved in 100 μL mobile phase A [98% dd$H_2O$, 2% acetonitrile (pH10) (Merck, Germany)], centrifuged at 14,000*g* for 20 minutes, and the supernatant was collected. A 400 μg enzymatic bovine serum albumin (BSA, Sigma-Aldrich, St. Louis, MO) was added to the column (Durashell-C18, 4.6 mm × 250 mm, 5 μm, 100 Å) (Agela, Wilmington, DE) to test the conditions of isolation (column temperature: 45°C, detection wavelength: 214 nm). Subsequently, 100 μL of the prepared sample was loaded at a flow rate of 0.7 mL/minute. The separation gradient was as follows: 0 minutes, 5% mobile phase B (98% acetonitrile, 2% dd$H_2O$, pH value of dd$H_2O$ was upregulated to 10 with ammonia); 5 minutes, 8% mobile phase B; 35 minutes, 18% mobile phase B; 62 minutes, 32% mobile phase B; 64 minutes, 95% mobile phase B; 68 minutes: 95% mobile phase B; and 72 minutes: 5% mobile phase B. Protein analyses were performed using nano-reverse-phase liquid chromatography connected to a Q-Exactive mass spectrometer (Thermo Scientific). Components isolated from high pH reversed-phase were redissolved with 20 μL [2% methanol (Sigma-Aldrich, St. Louis, MO), 0.1% formic acid (Sigma-Aldrich, St. Louis, MO)] and centrifuged at 12,000 rpm for 10 minutes. The supernatant was collected and loaded by the sandwich method in a volume of 10 μL and a flow rate of 350 nL/minute over 15 minutes for the loading pump. The flow rate of isolation was 350 nL/minute, with an isolation gradient as follows: 0 minutes, 4% mobile phase B (100% acetonitrile and 0.1% formic acid); 5 minutes, 15% mobile phase B; 40 minutes, 25% mobile phase B; 65 minutes, 35% mobile phase B; 70 minutes, 95% mobile phase B; 82 minutes, 95% mobile phase B; 85 minutes, 4% mobile phase B; and 90 minutes, 4% mobile phase B. The mass spectroscopy parameters were as follows: spray voltage 2.1 kV; capillary temperature 250°C, and full MS scanning range 350-1800 m/z.

### Bioinformatics Analysis

Peptide and protein identification were performed by searching the NCBI database (http://www.ncbi.nlm.nih.gov/protein?term=txid10114[Organism]) according to the species, completeness of database annotation and reliability of the sequences. In this study, the NCBI database (version: Refseq_txid10114 _20140412) and the rat species were selected. The iTRAQ mass analysis was performed using Thermo Q-Exactive spectrometry. The raw files (*.RAW) were processed using the Thermo supporting software Proteome Discoverer1.3. The search parameters were as follows: enzyme: trypsin; static modification: C carboxyamidomethylation (57.021 Da); dynamic modification: M oxidation (15.995 Da), N terminal, K, iTRAQ 4 plex; species: *Rattus norvegicus*; false discovery rate determination: false discovery rate of all peptide and protein identifications: $<1\%$; precursor ion mass tolerance: $\pm 15$ ppm; fragment ion mass tolerance: $\pm 20$ ppm; and max missed cleavages: 2. According to the *P* value of the raw data, the significance of upregulated and downregulated proteins in the PF model was screened with $P \leq 0.05$. Using an upregulated or downregulated differential multiplier $\geq 1.5$, they were listed in further bioinformatics analyses. The DEPs were subjected to comprehensive functional annotation to determine all the related functions using the Database for Annotation, Visualization and Integrated Discovery (http://david.abcc.ncifcrf.gov).[15] Proteins were classified according to the biological process, cellular components and molecular functions in GeneOntology (GO) notes. The classification and enrichment analyses of pathways were performed using the Kyoto Encyclopedia of Genes and Genomes (KEGG) pathway database.

### Detection of CYP1A1 Messenger RNA by qPCR

To further validate the alterations of the DEPs identified by proteomic analysis, we examined the existence of CYP1A1 in the lung tissues of the 2 groups by quantitative real-time polymerase chain reaction (qPCR). Briefly, the preparation of total RNA was conducted using the TRIzol Reagent (Invitrogen, Waltham, MA) according to manufacturer instructions; 1 μg of RNA samples was reverse transcribed by RevertAid First Strand cDNA Synthesis Kit (ThermoFisher Scientific, Waltham, MA) (200 U of reverse transcriptase per sample with 0.5 μg of random hexamer primers ). The messenger RNA transcript level of CYP1A1 was measured using the SYBR Premix Ex Taq II (Tli RNaseH Plus) kit (TaKaRa, Dalian, China). The PCR reaction mixtures (10 μL) contained 5.0 μL SYBR Premix Ex Taq II buffer

(2×), 0.5 μL complementary DNA template, 0.25 μL forward primer, 0.25 μL reverse primer and 4.0 μL dd$H_2O$. GAPDH gene was used as internal standard gene. qPCR analysis was performed by using the 7500 Fast Real-Time PCR System (Applied BioSystems, Foster City, CA) under the following cycling conditions: initial denaturation at 95°C for 30 seconds, then 40 cycles of denaturation at 95°C for 5 seconds and annealing at 60°C for 30 seconds. Each sample was analyzed in 2 parallel aliquots. The data were analyzed by the 5700 Sequence Detection System software (version 1.3, Applied Biosystems, Waltham, MA) and evaluated by the delta-delta Ct method to calculate the fold-change for relative quantitation of gene expression.

### Analysis of CYP1A1 by Western Blot in Rat Lung Tissues

For Western blot analysis, concentrations of the protein samples extracted from the rat tissues were determined by the Bradford method. Equal amounts of protein (20 μg protein per well) of each sample were separated by electrophoresis in a 12% SDS-polyacrylamide gel and electrotransferred onto a polyvinylidene difluoride membrane (Millipore, Bedford, MA). After blocking with 5% (w/v) nonfat milk in TBST (20 mM Tris-HCl, pH7.6, 136 mM NaCl and 0.1% Tween-20) for 1 hour at room temperature and rinsing, samples were immersed in 3% skim milk containing antibodies against CYP1A1 (polyclonal, Abcam, Cambridge, MA) and GAPDH (monoclonal sc-47724, Santa Cruz Biotechnology) overnight at 4°C. The membranes were then washed 4 times with TBST (5 minutes each) and incubated at room temperature for 1.5 hours with antigoat secondary horseradish peroxidase-conjugated antibody (1:2000, SC-2768, Santa Cruz, CA). After incubation with BeyoECL Plus (Beyotime Biotechnology, Nantong, China), the bands were visualized using ChemiDoc-It2 810 Imager (UVP) and quantified by densitometric analysis using image processing. For loading control, the blots were stripped and detected with a monoclonal anti-β-actin (1:2000, SC-2048, Santa Cruz, CA) antibody to normalize data as an internal standard.

### Statistical Analysis

SPSS17.0 statistical software was used to measure the data. The scores were expressed as $\bar{x} \pm s$, and the *t* test was performed. Changes in the same indexes among different groups were analyzed using 1-way analysis of variance, and $P < 0.05$ was considered to indicate statistical significance.

## RESULTS

### Microscopic Observation of Lung Tissue Pathology

As shown in Figure 1, the rat lung tissue in the control group was normal with occasionally visible inflammatory cells. However, rats in the model group showed disordered and severely damaged lung tissue with collapsed alveolar cavity, significantly widened alveolar septa, a large amount of fibrous tissue proliferation and collagen deposition, consolidation of alveoli and significant infiltration of inflammatory cells mostly showing grade 3 fibrosis and grade 2 alveolitis. The scores of alveolitis and PF were significantly increased in the model group compared with the control group ($P < 0.01$) (Table 1).

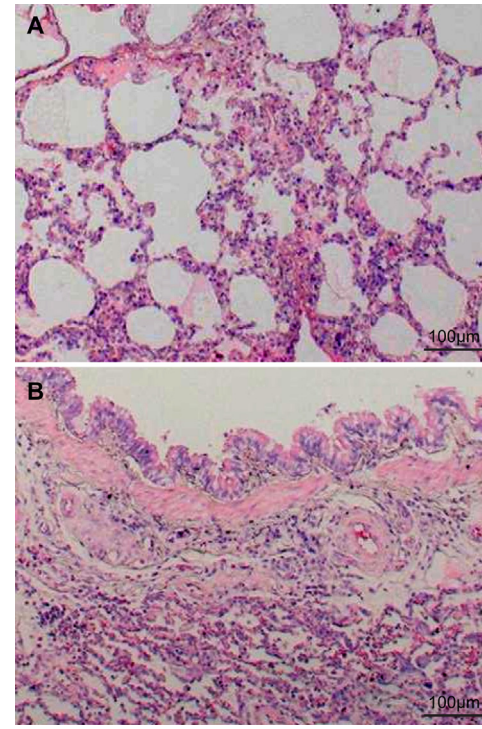


**FIGURE 1.** Histopathological changes of the lung tissues in rats by hematoxylin-eosin staining. (A) Normal control. (B) The rat pulmonary fibrosis.

### Effects of Bleomycin on Lung Coefficient and Hydroxyproline Content in Lung Tissue

As shown in Table 2, the lung coefficient and hydroxyproline content in lung tissue were significantly increased in the model group compared with the control group ($P < 0.05$), indicating significant differences in ECM deposition ($P < 0.01$ and 0.05). Excessive deposition of ECM is pathognomonic of PF. Collagen is the main component of ECM, whereas hydroxyproline is a unique amino acid of collagen. Abnormalities in collagen metabolism alter the

**TABLE 1.** Effects of bleomycin on alveolitis and PF in rat ($\bar{x} \pm s$).

| Group | Alveolitis score | PF score |
|---|---|---|
| Control group ($n = 8$) | 0.19 ± 0.56 | 0 |
| Model group ($n = 8$) | 1.60 ± 0.89 | 2.20 ± 0.45[a] |

[a] $P < 0.05$, compared with the control group.

**TABLE 2.** Effects of bleomycin on lung coefficient and hydroxyproline content ($\bar{x} \pm s$).

| Group | Lung coefficient (mg/g) | Hydroxyproline (mg/g) |
|---|---|---|
| Control group | 4.66 ± 0.59 | 0.72 ± 0.06 |
| Model group | 8.64 ± 1.27[a] | 1.11 ± 0.13[a] |

[a] $P < 0.01$, compared with the control group.

corresponding hydroxyproline content in the tissue. Thus, the hydroxyproline levels in the lung reflect the content of collagen, or ECM, in the lung tissue.

### Protein Identification and Differential Expression Analysis

In this study, rats with bleomycin-induced PF were subjected to proteomics analysis using iTRAQ combined with 2D LC-MS-MS techniques. Differential protein expression was determined at a ratio $\geq$ 1.5-fold and $P \leq 0.05$ in a single sample test according to the literature and system deviation. Totally, 146 DEPs were identified ($P \leq 0.05$) including 88 upregulated proteins and 58 downregulated proteins in the PF rat model group (Table 3).

The results of the present study showed that the expression of CYP1A1 messenger RNA in the rat model with PF was significantly reduced ($P < 0.05$, Figure 2A). As shown in Figure 2B and C, validation of the result by Western blot analysis revealed that the protein expression of CYP1A1 in the model PF group was significantly lower than that in the normal group ($P < 0.05$).

### Protein Cluster Analysis

Protein functions were clustered and biological processes were analyzed via GO. A total of 146 kinds of proteins were found to be mainly associated with inflammation, damage response, vitamin A synthesis and metabolism and other biological process. The main cellular components include platelets, secretory granules, vesicles and rough endoplasmic reticulum, which may be closely associated with an inflammatory reaction. All proteins were clustered into 6 KEGG pathways, namely lysosome pathway, extracellular matrix receptor interaction pathway, renin-angiotensin system pathway, hematopoietic cell lines pathway, tryptophan metabolic pathway and retinol metabolism pathway.

## DISCUSSION

Intratracheal perfusion of bleomycin causes PF in rats. As the best experimental tool available, the animal model with PF induced by bleomycin has been widely used to investigate the occurrence and development of PF and its mechanism.[16] The pathology is similar to that of idiopathic PF in humans. On day 3 after bleomycin treatment, the rat lungs started to display inflammation, including exudation of inflammatory cells, edema and widening of alveolar septum and significant increases in lung weight, lung coefficient and alveolar inflammation score compared with the control group. Inflammation was most significant on day 7. Fibroblasts were significantly increased and proliferated on day 14. PF was most remarkable on day 28.[17,18] Therefore, we used the samples of lung tissues obtained from the rat model of bleomycin-induced PF at 28 days to screen the underlying proteins related to PF.

Proteomic analysis provides new insights for understanding the molecular pathogenesis of PF.[19-21] For example, Fukunaga et al[20] conducted integrative microRNA microarray and iTRAQ-coupled LC-MS-MS proteomic analyses in the bleomycin rat model and found that alterations of microRNAs and proteins are associated with the early phase of bleomycin-induced pulmonary fibrosis. A dynamic proteomics platform via stable isotope labeling and LC-MS-based mass isotopomer analysis can be used for understanding altered ECM protein turnover associated with the onset and progression of fibrotic disease.[21] In this study, we performed iTRAQ coupled with LC-MS-MS to detect DEPs in lung tissues of the model. We found that the DEPs accumulated in the ECM receptor pathway. In PF, the ECM receptor expression is increased in interstitial cells, leading to the proliferation and differentiation of interstitial lung cells via signal transduction after ligand-receptor binding, further promoting the synthesis and secretion of fibronectin and collagen.[22,23] The KEGG pathway enrichment revealed accumulation of a large number of DEPs between the model and the control groups in the renin-angiotensin system. Angiotensin II upregulates the expression of cytokine transforming growth factor-β, stimulates fibroblast proliferation, transforms fibroblasts to myofibroblasts and extracellular matrix deposition, resulting in fibrosis.[24] Prostaglandin is synthesized from arachidonic acid *in vivo*[25] and promotes renin secretion. Lipoxygenase catalyzes arachidonic acid metabolism.[26] In this study, the lipoxygenases 12 and 15 were significantly decreased in the model group compared with the control group, which indicated that the increase in arachidonic acid may be due to reduced lipoxygenase expression, leading to renin secretion and increased generation of angiotensin II. These findings demonstrate that increased *in vivo* activity of lipoxygenase may reduce the degree of PF.

PF originates in the pulmonary alveoli, whereas alveolitis and the increased number of macrophages may be the early manifestation. In PF, pulmonary inflammatory cells, pulmonary epithelial cells and mast cells play a direct or indirect role by secreting cytokines, inflammatory mediators and other biologically active substances.[27] Cluster analysis of protein function suggested that many DEPs were associated with damage and defense response and inflammation. In addition, KEGG pathway enrichment revealed that a

**TABLE 3.** DEPs in the PF rat model / control group (M / C).

| Description | M/C | *P* Value |
|---|---|---|
| Alpha-1B-glycoprotein precursor [*R. norvegicus*] | 0.146 | 0.000 |
| PREDICTED: alpha-1B-glycoprotein [*R. norvegicus*] | 0.203 | 0.000 |
| Myelin protein P0 precursor [*R. norvegicus*] | 0.224 | 0.000 |
| Arachidonate 15-lipoxygenase [*R. norvegicus*] | 0.273 | 0.000 |
| Galectin-5 [*R. norvegicus*] | 0.297 | 0.000 |
| Platelet factor 4 precursor [*R. norvegicus*] | 0.331 | 0.000 |
| Platelet basic protein precursor [*R. norvegicus*] | 0.339 | 0.000 |
| Alpha-hemoglobin-stabilizing protein [*R. norvegicus*] | 0.339 | 0.000 |
| PREDICTED: integrin alpha-IIb [*R. norvegicus*] | 0.358 | 0.000 |
| PREDICTED: platelet glycoprotein V isoform X1 [*R. norvegicus*] | 0.375 | 0.000 |
| Platelet glycoprotein IX precursor [*R. norvegicus*] | 0.392 | 0.000 |
| Mitochondrial brown fat uncoupling protein 1 [*R. norvegicus*] | 0.392 | 0.000 |
| Mast cell protease 2 precursor [*R. norvegicus*] | 0.411 | 0.000 |
| Mast cell protease 8-like 2 precursor [*R. norvegicus*] | 0.413 | 0.000 |
| Granzyme-like protein 2 precursor [*R. norvegicus*] | 0.420 | 0.000 |
| Platelet glycoprotein Ib beta chain precursor [*R. norvegicus*] | 0.460 | 0.000 |
| Cytochrome P4501A1 [*R. norvegicus*] | 0.464 | 0.000 |
| Carbonic anhydrase 3 [*R. norvegicus*] | 0.470 | 0.000 |
| Integrin, beta 3 precursor [*R. norvegicus*] | 0.475 | 0.000 |
| PREDICTED: tubulin beta-1 chain isoform X1 [*R. norvegicus*] | 0.476 | 0.000 |
| Thrombospondin 1 precursor [*R norvegicus*] | 0.479 | 0.000 |
| Trafficking protein particle complex subunit 2-like protein [*R. norvegicus*] | 0.484 | 0.000 |
| PREDICTED: interferon-inducible GTPase 1-like [*R. norvegicus*] | 0.492 | 0.000 |
| Copine I [*R norvegicus*] | 0.496 | 0.000 |
| Retinal dehydrogenase 2 [*R norvegicus*] | 0.498 | 0.000 |
| Heart- and neural crest derivatives–expressed protein 2 [*R. norvegicus*] | 0.514 | 0.000 |
| Sushi domain–containing protein 2 precursor [*R. norvegicus*] | 0.515 | 0.000 |
| PREDICTED: multimerin-1 isoform X2 [*R. norvegicus*] | 0.517 | 0.000 |
| Platelet glycoprotein Ib alpha chain precursor [*R. norvegicus*] | 0.527 | 0.000 |
| Protein transport protein Sec31A [*R. norvegicus*] | 0.533 | 0.000 |
| Apolipoprotein A-II preproprotein [*R. norvegicus*] | 0.543 | 0.000 |
| PREDICTED: collagen alpha-3(IV) chain-like [*R. norvegicus*] | 0.547 | 0.000 |
| RT1 class I, locus M1, and gene 2 precursor [*R. norvegicus*] | 0.549 | 0.000 |
| Ubiquitin-60S ribosomal protein L40 [*R. norvegicus*] | 0.566 | 0.000 |
| Beta-defensin 4 precursor [*R. norvegicus*] | 0.582 | 0.000 |
| PREDICTED: immortalization upregulated protein [*R. norvegicus*] | 0.587 | 0.000 |
| Coagulation factor V [*R. norvegicus*] | 0.592 | 0.000 |
| Phosphatase and actin regulator 1 [*R. norvegicus*] | 0.598 | 0.000 |
| PREDICTED: arachidonate 12-lipoxygenase, 12S-type isoform X1 [*R. norvegicus*] | 0.604 | 0.000 |
| Calcitonin gene–related peptide type 1 receptor precursor [*R. norvegicus*] | 0.614 | 0.000 |
| Transmembrane protein 100 [*R. norvegicus*] | 0.615 | 0.000 |
| collagen alpha-1(XV) chain precursor [*R. norvegicus*] | 0.618 | 0.000 |
| PREDICTED: P-selectin isoform X1 [*R. norvegicus*] | 0.622 | 0.000 |
| PREDICTED: multidrug resistance protein 1 isoform X1 [*R. norvegicus*] | 0.625 | 0.000 |
| PREDICTED: rap guanine nucleotide exchange factor 6 isoform X9 [*R. norvegicus*] | 0.626 | 0.000 |
| PREDICTED: regulator of G-protein signaling 18 [*R. norvegicus*] | 0.628 | 0.000 |
| corticosteroid 11-beta-dehydrogenase isozyme 1 [*R. norvegicus*] | 0.635 | 0.000 |
| von Willebrand factor precursor [*R. norvegicus*] | 0.641 | 0.000 |
| RAS guanyl-releasing protein 2 [*R. norvegicus*] | 0.644 | 0.000 |
| PREDICTED: cGMP-specific 3',5'-cyclic phosphodiesterase isoform X1 [*R. norvegicus*] | 0.646 | 0.000 |
| PREDICTED: breakpoint cluster region protein [*R. norvegicus*] | 0.646 | 0.000 |
| plasmalemma vesicle–associated protein [*R. norvegicus*] | 0.648 | 0.000 |
| transferrin receptor protein 1 [*R. norvegicus*] | 0.649 | 0.000 |
| PREDICTED: uncharacterized protein LOC102549235 [*R. norvegicus*] | 0.651 | 0.000 |
| Retinal dehydrogenase 1 [*R. norvegicus*] | 0.653 | 0.000 |
| Fibrinogen-like 2 precursor [*R. norvegicus*] | 0.654 | 0.000 |
| Myc target protein 1 [*R. norvegicus*] | 0.657 | 0.000 |

*(continued on next page)*

**TABLE 3.** *(continued)*

| Description | M/C | *P* Value |
|---|---|---|
| 15-Hydroxyprostaglandin dehydrogenase [NAD(+)] [*R. norvegicus*] | 0.657 | 0.000 |
| N-acylethanolamine-hydrolyzing acid amidase precursor [*R. norvegicus*] | 1.501 | 0.000 |
| Transmembrane glycoprotein NMB precursor [*R. norvegicus*] | 1.502 | 0.000 |
| PREDICTED: MLV-related proviral Env polyprotein-like isoform X2 [*R. norvegicus*] | 1.502 | 0.000 |
| Galectin-3 [*R norvegicus*] | 1.507 | 0.000 |
| Microsomal triglyceride transfer protein large subunit precursor [*R. norvegicus*] | 1.513 | 0.000 |
| PREDICTED: serum amyloid A-3 protein [*R. norvegicus*] | 1.514 | 0.000 |
| PREDICTED: microfibril-associated glycoprotein 4-like isoform X2 [*R. norvegicus*] | 1.516 | 0.000 |
| Legumain precursor [*R. norvegicus*] | 1.516 | 0.000 |
| Fibromodulin precursor [*R. norvegicus*] | 1.517 | 0.000 |
| beta-sarcoglycan [*R. norvegicus*] | 1.518 | 0.000 |
| Macrosialin precursor [*R. norvegicus*] | 1.523 | 0.000 |
| Axonemal dynein light intermediate polypeptide 1 [*R. norvegicus*] | 1.524 | 0.000 |
| Nuclear autoantigen Sp-100 [*R. norvegicus*] | 1.528 | 0.000 |
| PREDICTED: RT1 class Ia, locus A2 isoform X1 [*R. norvegicus*] | 1.543 | 0.000 |
| Secreted frizzled-related protein 1 precursor [*R. norvegicus*] | 1.549 | 0.000 |
| PREDICTED: Ig kappa chain V19-17-like [*R. norvegicus*] | 1.552 | 0.000 |
| V-type proton ATPase 16 kDa proteolipid subunit [*R. norvegicus*] | 1.555 | 0.000 |
| PREDICTED: Ig lambda-1 chain C region isoform X2 [*R. norvegicus*] | 1.555 | 0.000 |
| PREDICTED: tetratricopeptide repeat protein 39A isoform X3 [*R. norvegicus*] | 1.563 | 0.000 |
| PREDICTED: fibrous sheath-interacting protein 2-like [*R. norvegicus*] | 1.570 | 0.000 |
| Prostaglandin E synthase [*R. norvegicus*] | 1.574 | 0.000 |
| Neutrophil gelatinase–associated lipocalin precursor [*R. norvegicus*] | 1.575 | 0.000 |
| Translocon-associated protein subunit gamma [*R. norvegicus*] | 1.576 | 0.000 |
| Lipopolysaccharide-binding protein precursor [*R. norvegicus*] | 1.580 | 0.000 |
| Thymosin beta-4 [*R. norvegicus*] | 1.581 | 0.000 |
| Dual oxidase 2 precursor [*R. norvegicus*] | 1.585 | 0.000 |
| Heme oxygenase 1 [*R. norvegicus*] | 1.590 | 0.000 |
| Histone deacetylase 4 [*R. norvegicus*] | 1.591 | 0.000 |
| Lysozyme C-1 precursor [*R. norvegicus*] | 1.592 | 0.000 |
| Cytochrome P450 2D1 [*R. norvegicus*] | 1.600 | 0.000 |
| Indolethylamine N-methyltransferase [*R. norvegicus*] | 1.604 | 0.000 |
| PREDICTED: keratin, type II cytoskeletal 6A-like isoform 1 [*R. norvegicus*] | 1.606 | 0.000 |
| PREDICTED: ferric-chelate reductase 1 [*R. norvegicus*] | 1.608 | 0.000 |
| Retinoic acid receptor responder (tazarotene induced) 1 precursor [*R. norvegicus*] | 1.609 | 0.000 |
| Group XV phospholipase A2 precursor [*R. norvegicus*] | 1.615 | 0.000 |
| PREDICTED: immunoglobulin lambda-like polypeptide 5-like isoform X1 [*R. norvegicus*] | 1.615 | 0.000 |
| PREDICTED: collagen alpha-3(VI) chain isoform X3 [*R. norvegicus*] | 1.618 | 0.000 |
| PREDICTED: protein FAM3A isoform X3 [*R. norvegicus*] | 1.622 | 0.000 |
| Cathepsin S preproprotein [*R. norvegicus*] | 1.628 | 0.000 |
| Cathepsin Z precursor [*R. norvegicus*] | 1.629 | 0.000 |
| rab-like protein 2A [*R. norvegicus*] | 1.631 | 0.000 |
| PREDICTED: 14-3-3 protein sigma [*R. norvegicus*] | 1.633 | 0.000 |
| Lumican precursor [*R. norvegicus*] | 1.642 | 0.000 |
| Polypeptide N-acetylgalactosaminyltransferase 3 [*R. norvegicus*] | 1.657 | 0.000 |
| Chitotriosidase-1 precursor [*R. norvegicus*] | 1.658 | 0.000 |
| Beta-Ala-His dipeptidase [*R. norvegicus*] | 1.671 | 0.000 |
| Collagen alpha-3(V) chain precursor [*R. norvegicus*] | 1.677 | 0.000 |
| PREDICTED: WD repeat-containing protein 17 isoform X7 [*R. norvegicus*] | 1.687 | 0.000 |
| Complement component 4, gene 2 precursor [*R. norvegicus*] | 1.697 | 0.000 |
| PREDICTED: uncharacterized protein LOC287059 isoform X1 [*R. norvegicus*] | 1.714 | 0.000 |
| Transmembrane protein 160 precursor [*R. norvegicus*] | 1.730 | 0.000 |
| PREDICTED: uncharacterized protein C8orf47 homolog isoform X2 [*R. norvegicus*] | 1.738 | 0.000 |
| PREDICTED: putative ciliary rootlet coiled-coil protein-like 3 protein-like [*R. norvegicus*] | 1.781 | 0.000 |
| PREDICTED: ovostatin homolog [*R. norvegicus*] | 1.795 | 0.000 |
| PREDICTED: DBF4-type zinc finger-containing protein 2 homolog isoform X3 [*R. norvegicus*] | 1.797 | 0.000 |

*(continued on next page)*

**TABLE 3.** *(continued)*

| Description | M/C | *P* Value |
|---|---|---|
| mast cell carboxypeptidase A precursor [*R. norvegicus*] | 1.798 | 0.000 |
| PREDICTED: Ig kappa chain V19-17-like [*R. norvegicus*] | 1.805 | 0.000 |
| PREDICTED: RT1 class Ia, locus A1 isoform X1 [*R. norvegicus*] | 1.848 | 0.000 |
| PREDICTED: uncharacterized protein LOC691828 [*R. norvegicus*] | 1.885 | 0.000 |
| PREDICTED: histone H2A type 2-A [*R. norvegicus*] | 1.888 | 0.000 |
| PREDICTED: ribosyldihydronicotinamide dehydrogenase [quinone] isoform X3 [*R. norvegicus*] | 1.934 | 0.000 |
| PREDICTED: Ig kappa chain V-III region MOPC 63 [*R. norvegicus*] | 1.975 | 0.000 |
| Protein FAM216A [*R. norvegicus*] | 1.990 | 0.000 |
| PREDICTED: uncharacterized protein LOC691718 [*R. norvegicus*] | 2.024 | 0.000 |
| Tryptase precursor [*R. norvegicus*] | 2.024 | 0.000 |
| PREDICTED: tartrate-resistant acid phosphatase type 5-like [*R. norvegicus*] | 2.054 | 0.000 |
| PREDICTED: immunoglobulin lambda-like polypeptide 5-like isoform X5 [*R. norvegicus*] | 2.083 | 0.000 |
| Acidic mammalian chitinase precursor [*R. norvegicus*] | 2.090 | 0.000 |
| Alpha-defensin 5, Paneth cell-specific precursor [*R. norvegicus*] | 2.143 | 0.000 |
| PREDICTED: ferritin heavy chain-like [*R. norvegicus*] | 2.249 | 0.000 |
| Chymase precursor [*R. norvegicus*] | 2.258 | 0.000 |
| PREDICTED: aldehyde dehydrogenase, mitochondrial isoform X1 [*R. norvegicus*] | 2.425 | 0.000 |
| Mast cell protease 1 preproprotein [*R. norvegicus*] | 2.505 | 0.000 |
| Aldehyde dehydrogenase, cytosolic 1 [*R. norvegicus*] | 2.548 | 0.000 |
| PREDICTED: immunoglobulin lambda-like polypeptide 5-like isoform X11 [*R. norvegicus*] | 2.563 | 0.000 |
| PREDICTED: Ig heavy chain V region IR2-like [*R. norvegicus*] | 2.766 | 0.000 |
| Keratin, type I cytoskeletal 14 [*R. norvegicus*] | 2.905 | 0.000 |
| Protein FAM65B [*R norvegicus*] | 2.985 | 0.000 |
| PREDICTED: LOW QUALITY PROTEIN: zinc finger protein 658-like [*R. norvegicus*] | 3.058 | 0.000 |
| Pancreatic secretory granule membrane major glycoprotein GP2 precursor [*R. norvegicus*] | 3.137 | 0.000 |
| Keratin, type II cytoskeletal 5 [*R. norvegicus*] | 3.365 | 0.000 |
| PREDICTED: mucin-5B [*R. norvegicus*] | 3.416 | 0.000 |
| Anterior gradient protein 2 homolog precursor [*R. norvegicus*] | 3.459 | 0.000 |
| Intelectin 1 (galactofuranose binding) precursor [*R. norvegicus*] | 3.496 | 0.000 |
| BPI fold-containing family B member 1 precursor [*R. norvegicus*] | 3.861 | 0.000 |
| PREDICTED: Ig lambda chain V-VI region EB4 isoform X1 [*R. norvegicus*] | 4.339 | 0.000 |
| PREDICTED: immunoglobulin lambda-like polypeptide 5-like isoform X10 [*R. norvegicus*] | 7.023 | 0.000 |
| PREDICTED: Ig lambda chain V-VI region EB4 isoform X2 [*R. norvegicus*] | 13.233 | 0.000 |

large number of DEPs accumulated in the lysosomal pathway, whereas cathepsin Z, cathepsin S and other proteins related to lysosome were also significantly upregulated. Furthermore, carboxypeptidase A and mast cell proteinase 1 were also significantly upregulated. These findings suggested that PF is associated with alveolitis, which is consistent with previous results. Thus, decreasing the activity of inflammatory cells and reducing the release of inflammatory mediators play an important role in reducing the degree of alveolitis, but also contribute to the early treatment of PF.

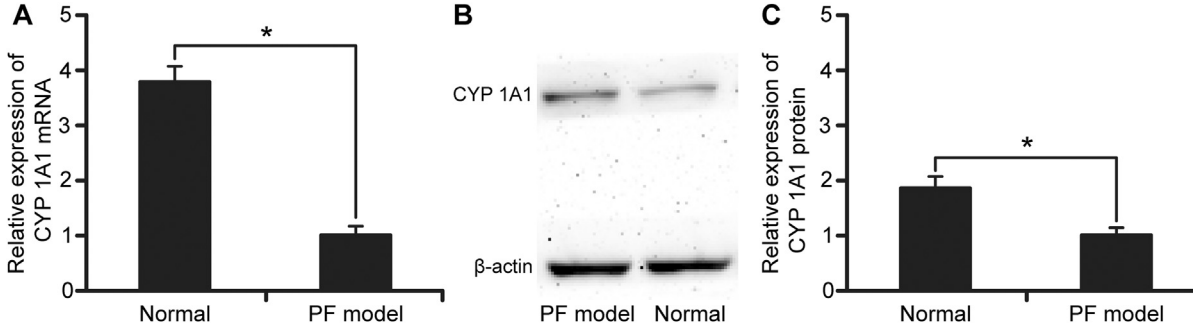


**FIGURE 2.** Expression of CYP 1A 1 mRNA and protein in the lung tissues of the rat PF model and the control groups detected by quantitative real-time polymerase chain reaction (qPCR) (A) and Western blot (B and C). mRNA, messenger RNA. $^{*}P < 0.05$, compared with the control group.

The KEGG pathway analysis revealed that DEPs were significantly concentrated in the retinol metabolic pathway. In addition, we also found that the expression of immunoglobulin was significantly upregulated in the model group, which might be associated with vitamin A. Vitamin A, also known as retinol, is closely associated with inflammatory response[28] and promotes the synthesis of immunoglobulin.[29] These findings indicate that vitamin A may mediate alveolitis via immunoglobulin synthesis, resulting in PF. Thus, immunoglobulin and vitamin A represent the likely indicators of early diagnosis in PF, but also play an important role in delaying its incidence.

A series of DEPs related to PF in this study were identified by iTRAQ technology, suggesting that the iTRAQ technology has a good prospect on the study of the pathogenesis and the biomarkers of PF. As a preliminary result, the numbers of the samples in this study are relatively small, so more samples are needed to verify these differential proteins identified in this study. Further study should be performed to clarify the role of these proteins involved in the occurrence and development of PF. For example, we found that CYP1A1 expression was significantly downregulated in the model group compared with the control group. *In vitro* study showed downregulation of CYP1A1 induction by tumor necrosis factor α and activated NF-κB.[30] Ghanem et al[31] reported that suppression of CYP2B1 and inducible CYP1A1 following CD and PAH exposure is associated with, but not caused by, upregulation of Bax expression and apoptosis of alveolar cells.

## CONCLUSIONS

In summary, we found that some proteins are closely relevant to the occurrence and development of PF using iTRAQ. The proteins expressed in bleomycin-induced PF rat model provide important data for further functional analysis of proteins involved in PF. The findings in this study indicated that iTRAQ is a useful technologic method in comparative proteomic study of multiple samples, which could figure out a dynamically quantitative expression pattern of proteins. In addition, the results also provided useful clues for further research to elucidate molecular mechanism of PF.

## REFERENCES


1. **Meltzer EB, Noble PW.** Idiopathic pulmonary fibrosis. Orphanet J Rare Dis 2008;3:8.
2. **Danoff SK, Terry PB, Horton MR.** A clinician's guide to the diagnosis and treatment of interstitial lung diseases. South Med J 2007;100:579–87.
3. **Coker RK, Laurent GJ.** Pulmonary fibrosis: cytokines in the balance. Eur Respir J 1998;11:1218–21.
4. **Flaherty KR, Thwaite EL, Kazerooni EA, et al.** Radiological versus histological diagnosis in UIP and NSIP: survival implications. Thorax 2003;58:143–8.
5. **King TE Jr, Tooze JA, Schwarz MI, et al.** Predicting survival in idiopathic pulmonary fibrosis: scoring system and survival model. Am J Respir Crit Care Med 2001;164:1171–81.
6. **Turner-Warwick M, Burrows B, Johnson A.** Cryptogenic fibrosing alveolitis: response to corticosteroid treatment and its effect on survival. Thorax 1980;35:593–9.
7. **Bringardner BD, Baran CP, Eubank TD, et al.** The role of inflammation in the pathogenesis of idiopathic pulmonary fibrosis. Antioxid Redox Signal 2008;10:287–301.
8. **Zhou Q, Chen T, Zhang W, et al.** Suppression of Von Hippel-Lindau Protein in fibroblasts protects against bleomycin-induced pulmonary fibrosis. Am J Respir Cell Mol Biol 2016;54:728–39.
9. **Adamson IY, Young L, Bowden DH.** Relationship of alveolar epithelial injury and repair to the induction of pulmonary fibrosis. Am J Pathol 1988;130:377–83.
10. **Kilic T, Parlakpinar H, Taslidere E, et al.** Protective and therapeutic effect of apocynin on bleomycin-induced lung fibrosis in rats. Inflammation 2015;38:1166–80.
11. **Choe LH, Aggarwal K, Franck Z, et al.** A comparison of the consistency of proteome quantitation using two-dimensional electrophoresis and shotgun isobaric tagging in *Escherichia coli* cells. Electrophoresis 2005;26:2437–49.
12. **Wu WW, Wang G, Baek SJ, et al.** Comparative study of three proteomic quantitative methods, DIGE, cICAT, and iTRAQ, using 2D gel- or LC-MALDI TOF/TOF. J Proteome Res 2006;5:651–8.
13. **Zhan H, Huang F, Ma W, et al.** Protective effect of ginsenoside Rg1 on bleomycin-induced pulmonary fibrosis in rats: involvement of caveolin-1 and TGF-β1 signal pathway. Biol Pharm Bull 2016;39:1284–92.
14. **Szapiel SV, Elson NA, Fulmer JD, et al.** Bleomycin-induced interstitial pulmonary disease in the nude, athymic mouse. Am Rev Respir Dis 1979;120:893–9.
15. **Huang da W, Sherman BT, Lempicki RA.** Systematic and integrative analysis of large gene lists using DAVID bioinformatics resources. Nat Protoc 2009;4:44–57.
16. **Mouratis MA, Aidinis V.** Modeling pulmonary fibrosis with bleomycin. Curr Opin Pulm Med 2011;17:355–61.
17. **Tashiro J, Elliot SJ, Gerth DJ, et al.** Therapeutic benefits of young, but not old, adipose-derived mesenchymal stem cells in a chronic mouse model of bleomycin-induced pulmonary fibrosis. Transl Res 2015;166:554–67.
18. **Sabry MM, Elkalawy SA, Abo-Elnour RK, et al.** Histolgical and immuno-histochemical study on the effect of stem cell therapy on bleomycin induced pulmonary fibrosis in albino rat. Int J Stem Cells 2014;7:33–42.
19. **Kypreou KP, Kavvadas P, Karamessinis P, et al.** Altered expression of calreticulin during the development of fibrosis. Proteomics 2008;8:2407–19.
20. **Fukunaga S, Kakehashi A, Sumida K, et al.** Integrative analyses of miRNA and proteomics identify potential biological pathways associated with onset of pulmonary fibrosis in the bleomycin rat model. Toxicol Appl Pharmacol 2015;286:188–97.
21. **Decaris ML, Gatmaitan M, FlorCruz S, et al.** Proteomic analysis of altered extracellular matrix turnover in bleomycin-induced pulmonary fibrosis. Mol Cell Proteomics 2014;13:1741–52.
22. **Munger JS, Huang X, Kawakatsu H, et al.** The integrin alpha v beta 6 binds and activates latent TGF beta 1: a mechanism for regulating pulmonary inflammation and fibrosis. Cell 1999;96:319–28.
23. **Terao M, Yang L, Matsumura S, et al.** A vitamin D analog inhibits Th2 cytokine- and TGFbeta-induced periostin production in fibroblasts: a potential role for vitamin D in skin sclerosis. Dermatoendocrinol 2015;7:e1010983.
24. **Guo W, Shan B, Klingsberg RC, et al.** Abrogation of TGF-beta 1-induced fibroblast-myofibroblast differentiation by histone deacetylase inhibition. Am J Physiol Lung Cell Mol Physiol 2009;297:L864–L870.
25. **Kim S, Jin Z, Lee G, et al.** Prostaglandin potentiates 5-HT responses in stomach and ileum innervating visceral afferent sensory neurons. Biochem Biophys Res Commun 2015;456:167–72.

26. **Duchez AC, Boudreau LH, Bollinger J, et al.** Platelet microparticles are internalized in neutrophils via the concerted activity of 12-lipoxygenase and secreted phospholipase A2-IIA. Proc Natl Acad Sci U S A 2015;112:E3564–73.
27. **Xie L, Zhou D, Xiong J, et al.** Paraquat induce pulmonary epithelial-mesenchymal transition through transforming growth factor-beta1-dependent mechanism. Exp Toxicol Pathol 2016;68:69–76.
28. **Thurnham DI.** Inflammation and Vitamin A. Food Nutr Bull 2015;36:290–8.
29. **Fan X, Liu S, Liu G, et al.** Vitamin A deficiency impairs mucin expression and suppresses the mucosal immune function of the respiratory tract in chicks. PLoS One 2015;10:e0139131.
30. **Tian Y, Ke S, Chen M, et al.** Interactions between the aryl hydrocarbon receptor and P-TEFb. Sequential recruitment of transcription factors and differential phosphorylation of C-terminal domain of RNA polymerase II at cyp1a1 promoter. J Biol Chem 2003;278:44041–8.
31. **Ghanem MM, Battelli LA, Mercer RR, et al.** Apoptosis and Bax expression are increased by coal dust in the polycyclic aromatic hydrocarbon-exposed lung. Environ Health Perspect 2006;114:1367–1373.



From the Department of Urology (TY, BQ), The First Affiliated Hospital of Zhengzhou University, Zhengzhou, Henan, PR China; Department of Urology (TY, YM) and Department of Oncology (XC), The Affiliated Cancer Hospital of Zhengzhou University, Zhengzhou, Henan, PR China; Pharmacy College (YJ), Xinxiang Medical University, Xinxiang, Henan, PR China; Department of Oncology (LC), The Second Affiliated Hospital of Zhengzhou University, Zhengzhou, Henan, PR China.



Submitted July 1, 2016; accepted November 15, 2016.

The first 2 authors (TY, YJ) contributed equally to this work.

The authors declare that they have no conflict of interest.

This work was partly supported by the National Natural Science Foundation of China (grant No. 81172240/H1615) and the Key Science and Technology Project of Henan Province (122102310200).



Corresponding author: Baoping Qiao, MD, Department of Urology, The First Affiliated Hospital of Zhengzhou University, Zhengzhou, Henan, PR China (E-mail: 2542015600@qq.com).